Full-potential embedding for surfaces and interfaces

1992 J. Phys.: Condens. Matter 4 1475

(http://iopscience.iop.org/0953-8984/4/6/012)

J. Phys.: Condens. Matter 4 (1992) 1475–1488. Printed in the UK

Full-potential embedding for surfaces and interfaces

S Crampin, J B A N van Hoof, M Nekovee and J E Inglesfield
Institute for Theoretical Physics, Catholic University of Nijmegen, Toernooiveld, NL-6525ED Nijmegen, The Netherlands

Received 22 August 1991

Abstract. We extend the surface-embedded Green function technique for calculating the electronic structure of surfaces and interfaces by presenting a method for determining substrate embedding potentials which makes no approximations to the substrate potential. We first present an alternative derivation of the surface-embedded Green function method, to clarify the use of a planar surface in simulating embedding on a more complicated surface, and illustrate this with rigorous tests. Considering the case of a region embedded on two surfaces, we determine the conditions under which the resulting Green function may itself be used as a substrate-embedding potential, and thereby derive a procedure for obtaining an embedding potential which makes no approximation to the substrate potential. In the case of a substrate with semi-infinite periodicity this reduces to a self-consistency relation, for which we describe a first-order iterative solution. Finally, a particularly efficient scheme for obtaining local properties within a surface or interface region is outlined. This constitutes a full-potential solution to the one-electron Schrödinger equation for systems of two-dimensional periodicity, whose calculation time scales linearly with the number of atomic planes.

1. Introduction

Calculations of surface or interface electronic structure fall broadly into two categories, those which correctly treat the semi-infinite substrate or substrates, and those which employ slab or supercell boundary conditions. In the latter, a surface is unphysically located in the vicinity of other surfaces, either across a region of vacuum and/or a finite number of atomic layers, but they have the benefit that conventional band structure techniques may be used. Indeed, they have achieved considerable success in the description of various surface properties, such as work functions, total energies, atomic reconstructions and magnetism, but their ability to describe individual states for comparison with surface spectroscopies such as photoemission is less well established. Wavefunctions are far more sensitive to boundary conditions than integrated quantities such as charge densities and total energies, and may interact significantly over many atomic planes. In addition, both slab and supercell provide a poor description of the bulk continuum. The deficiencies of the slab or supercell boundary conditions become more acute when surfaces or interfaces with high Miller indices are considered, such as stepped surfaces and grain-boundaries, systems of importance to areas of catalysis and mechanical behaviour. The short interlayer separation requires the inclusion of a prohibitively large number of atoms in order to prevent interaction between neighbouring surfaces.

0953-8984/92/061475+14$04.50

Techniques which provide a correct description of the transition from surface to bulk are usually based upon the Green function and include multiple scattering methods such as layer Korringa–Kohn–Rostoker (LKKR) (MacLaren *et al* 1989), where the semi-infinite substrate is incorporated via a reflection matrix which describes the scattering of electrons; tight-binding formulations which exploit the short-range nature of the overlap integrals (Pollmann and Pantelides 1978); the Green-function linear-muffin-tin-orbitals method (GF-LMTO) (Skriver and Rosengaard 1991) in which structure constants within the tight-binding representation are short-ranged; and the surface-embedding Green function method (SEGF) (Inglesfield and Benesh 1988). The SEGF method provides a full-potential solution of the Schrödinger equation within a limited region of space (containing the surface or interface), and the influence of the semi-infinite substrate is incorporated via an energy-dependent non-local embedding potential which ensures the surface wavefunctions match correctly to bulk solutions. The embedding potential is a property of the substrate and need only be evaluated once for a given substrate direction (e.g. (111), (110), ...), but the energy dependence prevents linearization (in common with the LKKR and GF-LMTO methods). However, only one or two atomic layers are normally required to model a metal surface—considerably fewer than for slab or supercell techniques in which the interaction between neighbouring surfaces must be kept to a minimum—and so in addition to the improved accuracy, the SEGF technique can be a computationally efficient approach to determining the electronic structure of the surface and interfaces.

The embedding potential can be related to the reflection properties of the substrate. In previous applications this relationship has been used to determine the embedding potential for a semi-infinite 'muffin-tin' substrate, in which the potential within the substrate is approximated by the spherical average within non-overlapping spheres centred upon the atomic sites and the volume average in the interstitial. The reflection matrix may then be determined by the well-known techniques of LKKR or low-energy electron diffraction theory (Pendry 1974). Whilst this provides an extremely convenient method for determining the embedding potential, the limitations are obvious in that however accurate the solution obtained within the surface or interface region, it is limited by errors in the embedding potential. The inherent difficulties become more severe the less close-packed the substrate is. An additional problem arises from the incompatibility of surface and substrate potentials, which can result in artificial charge transfer which reduces the stability of the self-consistent iteration scheme. Moreover, this can lead to spurious shifts in the determined position of surface states relative to bulk band edges.

In this article we describe a new approach by which the substrate embedding potential may be determined with an accuracy comparable to that achieved in the surface or interface region. Since the embedding potential need only be determined once, and subsequently read in when the surface potential is being iterated, we initially provide a justification for the use of an embedding *plane* to simulate embedding on a more complicated surface. This permits a simple representation of the embedding potential which is independent of the surface region, and requires significantly less memory storage than the use of a non-planar embedding surface. We then indicate how the embedding potential for an arbitrary stacking of atomic planes may be constructed and present an efficient algorithm for generating the embedding potential of a substrate with semi-infinite periodicity. Finally, we conclude with some remarks on how local properties within the surface or interface may be most efficiently determined.

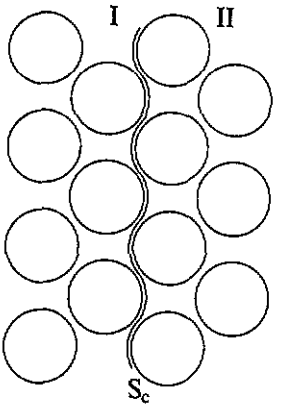

Figure 1. The region of interest (I) is separated from the substrate (II) by surface S_C.

2. Embedding on a plane

We begin this section by briefly summarizing the previous derivation of the SEGF method (Inglesfield and Benesh 1988), before providing an alternative derivation which clarifies the use of a plane embedding surface to simulate the true embedding plane.

Consider a trial function $\phi(\boldsymbol{r})$ in region I (figure 1), the region of interest. This is extended into the substrate (region II) with $\psi(\boldsymbol{r})$, an exact solution of the Schrödinger equation at energy ε, which matches in amplitude to ϕ over S_C, the surface which divides regions I and II. The expectation value of the Hamiltonian, which includes contributions from the discontinuity in the wavefunction derivative on S_C, is

$$E = \frac{\int_I \mathrm{d}^3\boldsymbol{r}\phi^* H\phi + \int_{II} \mathrm{d}^3\boldsymbol{r}\psi^* H\psi + \frac{1}{2}\int_{S_C} \mathrm{d}^2\boldsymbol{r}_s\,(\phi^*\partial\phi/\partial n_s - \psi^*\partial\psi/\partial n_s)}{\int_I \mathrm{d}^3\boldsymbol{r}\phi^*\phi + \int_{II} \mathrm{d}^3\boldsymbol{r}\psi^*\psi} \tag{1}$$

where n_s is the surface normal (from I to II). The substrate wavefunction ψ may be eliminated from (1) by introducing G_0^{-1}, the surface-inverse of the bulk Green function at energy ε with zero normal derivative on S_C (Inglesfield 1981). Minimizing with respect to variations in ε gives $\varepsilon = E$ and

$$E = \frac{\int_I \mathrm{d}^3\boldsymbol{r}\phi^* H\phi + \frac{1}{2}\int_{S_C} \mathrm{d}^2\boldsymbol{r}_s\phi^*\partial\phi/\partial n_s + \int_{S_C} \mathrm{d}^2\boldsymbol{r}_s \int_{S_C} \mathrm{d}^2\boldsymbol{r}'_s\phi^* G_0^{-1}\phi}{\int_I \mathrm{d}^3\boldsymbol{r}\phi^*\phi}. \tag{2}$$

Considering variations in ϕ, E is found to be stationary when

$$H\phi = E\phi \qquad \boldsymbol{r} \text{ in region I} \tag{3}$$

and

$$\frac{\partial\phi(\boldsymbol{r}_s)}{\partial n_s} = -2\int_{S_C} \mathrm{d}^2\boldsymbol{r}'_s G_0^{-1}(\boldsymbol{r}_s, \boldsymbol{r}'_s)\phi(\boldsymbol{r}'_s) \qquad \boldsymbol{r}_s \text{ on } S_C \tag{4}$$

i.e. ϕ satisfies the Schrödinger equation and has the correct logarithmic derivative on S_C to match smoothly to a bulk solution at energy E.

By expanding ϕ in a basis and minimizing E with respect to variations in the coefficients, one obtains an effective Schrödinger equation whose solution yields the electronic structure. All information regarding the substrate enters through G_0^{-1}, the embedding potential, evaluated over S_C. However, this causes some problems when it comes to implementing the method in a particular basis, through difficulties in evaluating the surface integrals. A surface which respects the partitioning between substrate and surface atoms contains concave and convex sections where it curves around the muffin-tins (figure 2), whereas a plane surface, which permits a simple representation of the embedding potential, cuts through substrate muffin-tins, requiring the inclusion of substrate caps within the region I, and/or cuts through surface atoms, requiring the omission of surface atom caps. Inglesfield and Benesh (1988) argued that it is possible to *transfer* the boundary condition contained in G_0^{-1} from the complicated surface which avoids cutting through muffin-tin spheres to a simpler planar surface, by integrating through constant potential between the original surface and the new surface. We now show that this is indeed possible and show how the resulting embedding potential is obtained.

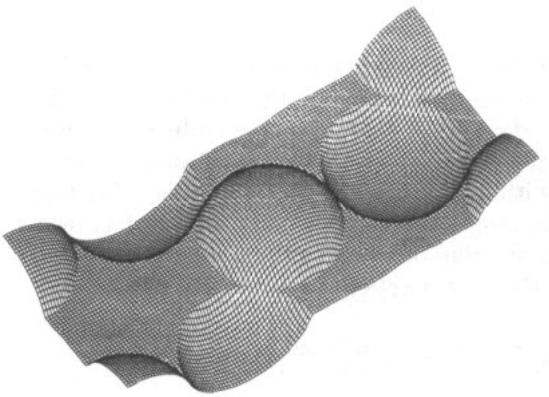

Figure 2. An embedding surface, in this case for FCC (210), which respects the partitioning of atoms into surface and substrate atoms in general consists of convex and concave caps due to protruding muffin-tins. Transferring the boundary condition from this complicated surface to a flat surface is greatly beneficial.

To do this we consider embedding our region of interest, I, onto free space, and determine under what conditions our trial solution ϕ is a solution of the Schrödinger equation within I with the correct boundary condition on S_C, the curvy surface, when the embedding surface is S, a plane. S_C separates regions I and Δ, and S represents regions Δ and II; in region Δ we take the potential to be zero (figure 3). Let us define our trial solution within $I + \Delta$ and match on S to χ, a solution of the free-electron Schrödinger equation at energy ε. As above the expectation value of the Hamiltonian is

$$E = \frac{\int_{I+\Delta} d^3\boldsymbol{r}\,\phi^* H\phi + \int_{II} d^3\boldsymbol{r}\,\chi^* H_0\chi + \frac{1}{2}\int_S d^2\boldsymbol{r}_s\,(\phi^*\partial\phi/\partial n_s - \chi^*\partial\chi/\partial n_s)}{\int_{I+\Delta} d^3\boldsymbol{r}\,\phi^*\phi + \int_{II} d^3\boldsymbol{r}\,\chi^*\chi} \tag{5}$$

If G_F is the free-electron Green function with zero normal derivative on S, so that (Inglesfield 1981)

$$\frac{\partial\chi(\boldsymbol{r}_s)}{\partial n_s} = -2\int_S d^2\boldsymbol{r}_s' G_F^{-1}(\boldsymbol{r}_s, \boldsymbol{r}_s')\chi(\boldsymbol{r}_s') \qquad \boldsymbol{r}_s \text{ on } S \tag{6}$$

minimizing (5) with respect to variations in ε gives

$$E = \frac{\int_{I+\Delta} d^3\boldsymbol{r}\ \phi^* H\phi + \frac{1}{2}\int_S d^2\boldsymbol{r}_s\ \phi^*\partial\phi/\partial n_s + \int_S d^2\boldsymbol{r}_s\ \int_S d^2\boldsymbol{r}'_s\ \phi^* G_F^{-1}\phi}{\int_{I+\Delta} d^3\boldsymbol{r}\ \phi^*\phi}. \tag{7}$$

Varying ϕ, we find the energy is stationary when $H\phi = E\phi$ for $\boldsymbol{r}$ in region $I + \Delta$ and ϕ has the same logarithmic derivative on S as χ.

$$\frac{\partial\phi(\boldsymbol{r}_s)}{\partial n_s} = -2\int_S d^2\boldsymbol{r}'_s\ G_F^{-1}(\boldsymbol{r}_s, \boldsymbol{r}'_s)\phi(\boldsymbol{r}'_s) \qquad \boldsymbol{r}_s \text{ on } S. \tag{8}$$

We now note that in region Δ both ϕ and χ satisfy the free-electron Schrödinger equation. Thus, since they possess the same amplitude and derivative on S, they will possess the same amplitude and derivative on S_C. Hence, if we construct our free-electron solution χ to have the same logarithmic derivative as an exact bulk solution on S_C, on S it will have the necessary logarithmic derivative to ensure that ϕ too has the correct logarithmic solution on S_C. Since our trial solution also satisfies the Schrödinger equation in region I, it is by construction the solution we desire.

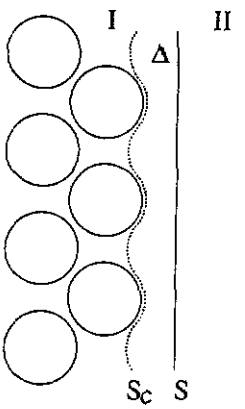

Figure 3. Embedding the region of interest (I) onto a free-electron solution over surface S, with zero potential in the volume Δ between S and the true embedding surface, S_C. The conditions under which the trial solution has the correct boundary conditions over S_C lead to a prescription for determining the embedding potential on S.

In the case of a substrate in which the true crystal potential is approximated by the muffin-tin form in the (infinitesimal) region of zero potential between atoms of different layers (and in particular on surface S_C which curves around muffin-tins) a bulk wavefunction with wavevector $\boldsymbol{k}_\parallel$ may be written as

$$\begin{aligned} \psi(\boldsymbol{r}) &= \sum_{\boldsymbol{g}} \psi_{\boldsymbol{g}}(z) e_{\boldsymbol{g}}(\boldsymbol{r}_\parallel, \boldsymbol{k}_\parallel) \qquad e_{\boldsymbol{g}}(\boldsymbol{r}_\parallel, \boldsymbol{k}_\parallel) = \frac{1}{\sqrt{A}} \exp\left[i(\boldsymbol{g} + \boldsymbol{k}_\parallel)\cdot\boldsymbol{r}_\parallel\right] \\ \psi_{\boldsymbol{g}}(z) &= \sum_{\boldsymbol{g}'} \left[\delta_{\boldsymbol{g}\boldsymbol{g}'} \exp(ik_{\boldsymbol{g}z} z) + R_{\boldsymbol{g}\boldsymbol{g}'} \exp(-ik_{\boldsymbol{g}z} z)\right] a_{\boldsymbol{g}'} \end{aligned} \tag{9}$$

where $k_{gz} = \sqrt{2E - |g + k_\parallel|^2}$ and $R_{gg'}$ is the reflection matrix of the semi-infinite half-space. Since this is also a solution of the free-electron Schrödinger equation at energy E, if we continue this definition into the muffin-tin spheres and use this for χ, then our free-electron solution has the same logarithmic derivative on any surface within the interstitial as the bulk wavefunction. If we assume the origin $z = 0$ is on the embedding plane, then from (6) we can construct the $k_\parallel$-resolved embedding potential

$$G^{-1}_{F,k_\parallel}(r_\parallel, r'_\parallel) = \sum_{gg'} (G^{-1}_{F,k_\parallel})_{gg'} e_g(r_\parallel, k_\parallel) e^*_{g'}(r'_\parallel, k_\parallel)$$
$$(G^{-1}_{F,k_\parallel})_{gg'} = -\frac{ik_{gz}}{2}\left[(1-R)(1+R)^{-1}\right]_{gg'}. \tag{10}$$

This is the expression given by Inglesfield and Benesh (1988).

It is relatively easy to show by matching Green functions that equation (10) represents an expansion on surface S of the surface-inverse of the free-space Green function with zero normal-derivative boundary conditions (on S) which, integrated through to S_C, coincides with the substrate Green function on this surface. Since both this Green function and our trial function satisfy the same differential equation within Δ, satisfying the modified boundary condition on S is entirely equivalent to satisfying the original boundary condition on S_C. Note that (9) is in fact a valid representation of a wavefunction outside any substrate (subject to in-plane periodicity requirements) truncated and matched onto free-space, so this argument is valid for general potentials.

In figure 3 we have considered the case when plane S lies entirely on the substrate side of surface S_C. In actual fact such a restriction is not necessary, and, for example, the plane S may be taken to be entirely on the surface side of S_C. Re-writing (7) as

$$E = \frac{\int_I d^3r \phi^* H \phi + \int_\Delta d^3r \phi^* H_0 \phi + \frac{1}{2}\int_S d^2r_s \phi^* \partial\phi/\partial n_s + \int_S d^2r_s \int_S d^2r'_s \phi^* G_F^{-1} \phi}{\int_I d^3r \phi^* \phi + \int_\Delta d^3r \phi^* \phi} \tag{11}$$

to distinguish integration volumes, we note that when S is not entirely on the substrate side of S_C, Δ and I overlap in this case. However, since we are attempting to minimize (11), we are free to use different expansions of the trial function for Δ and I. Thus within I, which includes the contribution from the atomic potentials, we can use the conventional linearized augmented plane-wave basis (LAPW) with an expansion in solutions of the atomic Schrödinger equation within the muffin-tins, whilst in Δ, and on surface S, we can use the plane wave component of the LAPW. The resulting matrix elements are then particularly easy to determine.

To demonstrate the validity of the use of a plane embedding surface, we consider the case of an internal interface, a Cu/Ni/Cu (100) monolayer sandwich (figure 4). Embedding an internal interface is essentially the two-surface generalization of the previous analysis (Farquhar and Inglesfield 1989). The effective Schrödinger equation is obtained by minimizing (cf (7))

$$E = \Bigg[\int_{I+\Delta^L+\Delta^R} d^3r \phi^* H \phi + \frac{1}{2}\int_{S^L} d^2r_s \phi^* \partial\phi/\partial n_s + \frac{1}{2}\int_{S^R} d^2r_s \phi^* \partial\phi/\partial n_s$$
$$+ \int_{S^L} d^2r_s \int_{S^L} d^2r'_s \phi^* G_L^{-1} \phi$$

$$+\int_{S^R} d^2r_s \int_{S^R} d^2r'_s \phi^* G_R^{-1} \phi \Big] \Big/ \int_{I+\Delta^L+\Delta^R} d^3r \phi^* \phi \tag{12}$$

where Δ^L (Δ^R) is the volume between the curvy embedding surface S_C^L (S_C^R) and the embedding plane S^L (S^R). G_L^{-1} and G_R^{-1} are the embedding potentials of the left and right half-spaces which produce the correct logarithmic derivative on the true embedding surfaces. We expand ϕ in an LAPW basis ($\chi_i(r; k_\parallel)$) and by varying the coefficients to minimize E, obtain an effective Schrödinger equation. The corresponding Green function is given at energy E by

$$G(r, r'; k_\parallel) = \sum_{i,j} \mathcal{G}_{ij}(k_\parallel) \chi_i(r; k_\parallel) \chi_j^*(r'; k_\parallel) \tag{13}$$

where the matrix of coefficients is given by

$$\begin{aligned} \mathcal{G} &= \left[H + C_{S^L}^\dagger (G_{L,k_\parallel}^{-1}) C_{S^L} + C_{S^R}^\dagger (G_{R,k_\parallel}^{-1}) C_{S^R} - EO \right]^{-1} \\ H_{ij} &= \int_{I+\Delta^L+\Delta^R} d^3r \chi_i^* H \chi_j + \frac{1}{2} \int_{S^L} \chi_i^* \frac{\partial \chi_j}{\partial n_s} + \frac{1}{2} \int_{S^R} \chi_i^* \frac{\partial \chi_j}{\partial n_s} \\ (C_S)_{gi} &= \int_s d^2r_s e_g^* \chi_i \qquad O_{ij} = \int_{I+\Delta^L+\Delta^R} d^3r \chi_i^* \chi_j \,. \end{aligned} \tag{14}$$

The density of states is determined by integrating throughout the muffin-tin spheres the charge density, obtained from $\varrho(r; k_\parallel) = \mathrm{Im} G(r, r; k_\parallel)/\pi$. Figure 5 shows a comparison of the density of states within the Ni muffin-tin evaluated using the above formalism, with various positions of the embedding planes, and that determined by the LKKR method (see MacLaren *et al* (1989) for further details of this part of the calculation) using an identical potential. We have used muffin-tin potentials for this comparison, bulk Cu potentials in the Cu substrate right up to the interface and a bulk Ni potential within the Ni monolayer. As in the conventional KKR method of band structure theory, the LKKR code uses a free space expansion within the interstitial and is thus exact for potentials of the muffin-tin form, spherically symmetric within non-overlapping spheres, zero elsewhere. The embedded Green function technique should be exact for all forms of potential, and so we expect both methods to produce comparable results. Despite the completely different approaches employed by the two methods, the LKKR results and those using embedding are in excellent agreement, indicating the validity of the use of a plane embedding surface. Note that we are comparing the muffin-tin density of states. By moving the embedding planes, the total density of states within the embedded region as a whole varies by virtue of the variation in the volume, but the contribution from the muffin-tin is constant. The remaining differences are numerical (for example, the two codes use different radial tabulations of the potentials) and finite basis sets. (The LKKR calculations used 29 g vectors and ℓ up to 3; the LAPW basis consisted of 160 vectors, angular momentum expansions to $\ell = 8$ and the embedding potential was expanded with 29 reciprocal lattice vectors.)

Our experience is that this degree of agreement does not extend indefinitely as the embedding planes are moved either toward the substrate or the Ni monolayer. In both cases differences appear at specific energy regions which increase as the embedding plane approaches the atomic planes. Those elements of the embedding potential which

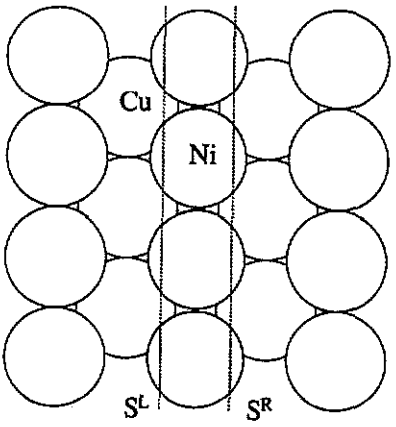

Figure 4. The embedding of a (100) Ni monolayer in Cu. The Cu substrates are replaced by embedding potentials on the planes S_L and S_R. For the examples described in the text, the planes cut through both Ni and Cu muffin tins.

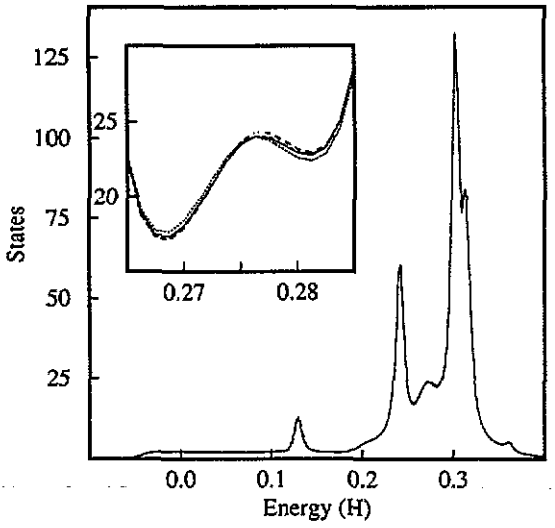

Figure 5. Muffin-tin density of states at $k_{\parallel} = (0,0)$ (per spin-Hartree) for a (100) Cu/Ni/Cu sandwich. Four curves are plotted. The full curve is the LKKR results. The broken curves are calculated with the embedded Green function method with the embedding planes at (short dash to long) 0.50, 0.55 and 0.60 times the interlayer separation. The results show remarkable agreement, as is evident from the inset which shows a section of the curve in detail. The density of states calculated within the varying embedded region as a whole differs by as much as 30% between the different embedding plane calculations. The energy contained an imaginary component of 0.005 H.

correspond to g with $|g + k_{\parallel}|^2 > 2E$ vary exponentially with changes in the position of the embedding plane, and not only does the number of basis vectors required in the expansion (10) rapidly increase but errors increase due to the integration back and forth from the embedding plane to the embedding surface. It is evident from figure 4 that for an interface between materials of similar atomic size, an embedding plane midway between atomic planes minimizes the distance over which the boundary

condition is transferred, and other than to demonstrate the validity of the embedding procedure there is little need to consider alternative embedding positions.

One further problem, also occurring for general potentials, arises from the poor behaviour of the g basis for the expansion of the embedding potential as the interlayer separation decreases. This is analogous to the difficulties experienced with the LKKR technique in similar situations, where the g basis is used as an intermediate expansion of the propagator connecting sites in different layers. The importance of additional basis vectors decreases exponentially at a rate dependent upon the interlayer spacing *and* $|g|$; since small interlayer spacings generally correspond to large reciprocal lattice meshes, the problems are particularly acute, and may only be overcome by using an alternative expansion basis for the problematic terms. Here, the solution is to augment the surface plane wave expansion (10) with additional functions.

3. Full-potential embedding

We now consider how to determine a substrate embedding potential which goes beyond the muffin-tin approximation. As mentioned previously, the accuracy of solution within the surface or interface is limited by the errors present in the embedding potential. Although screening lengths within metals are sufficiently short for the effects of these errors to be small, the materials which may be studied are largely restricted to those which have a relatively close-packed crystal structure. Even then, the anisotropy of the charge distribution within the vicinity of the embedding plane can be underestimated due to matching onto a muffin-tin potential, and a small degree of charge transfer between the substrate and embedded region, due to the incompatible potentials, can result in decreased stability during the self-consistent iterations and shifts in the location of surface/interface states.

It was established in the previous section that it is possible to embed on a plane surface and take matrix elements of the embedding potential with the plane wave component of the LAPW when the embedding potential is obtained from the substrate Green function, integrated through zero potential between the curvy embedding surface which avoids cutting muffin-tins and the embedding plane, and which has zero-normal derivative on this plane. Consider the right half-space. Given an embedding potential, $G^{-1}_{\mathrm{R},\boldsymbol{k}_\parallel}$, we can add on an additional volume I and determine the Green function, G, using equations (13) and (14), where we leave $G^{-1}_{\mathrm{L},\boldsymbol{k}_\parallel}$ unspecified at present. This Green function is the projection within I of the Green function which satisfies the full Schrödinger equation within I + substrate, and the free-electron Schrödinger equation within Δ^{L}. The presence of $G^{-1}_{\mathrm{L},\boldsymbol{k}_\parallel}$ acts as a second boundary condition on G, constraining the normal derivative. Therefore, if we specify $G^{-1}_{\mathrm{L},\boldsymbol{k}_\parallel} = 0$ on surface S^{L}, G is the Green function for I + substrate which has zero normal-derivative boundary condition on S^{L}, and G^{-1} is therefore an embedding potential for I + substrate. If we add an additional volume, I′, so that S'^{R} and Δ'^{R} are coincident with the previous surface S^{L} and volume Δ^{L}, the zero normal-derivative boundary condition integrated from S'^{R} through Δ'^{R} results in the same boundary condition on $S'^{\mathrm{R}}_{\mathrm{C}} = S^{\mathrm{L}}_{\mathrm{C}}$ as was integrated through Δ^{L} to give it. Thus the resulting Green function is smooth and continuous over all I′ + I + substrate and satisfies the Schrödinger equation in that volume. This procedure can then be repeated, the embedding potential describing the original substrate plus the additional volumes. If a muffin-tin substrate was employed

originally, adding regions in which a full potential description of the potential of the same material is used will decrease the errors in the embedding potential. Alternatively, starting from some arbitrary embedding potential, the zero matrix for example, and repeatedly adding identical volumes representing substrate atomic planes till convergence, will generate a full potential substrate embedding potential.

To see how this works in practice, we expand the Green function (13) on surface S^{L} when $G^{-1}_{\mathrm{L},k_\parallel} = 0$ and invert to give the new embedding potential for the substrate plus one additional layer:

$$\begin{aligned} G^{-1}_{k_\parallel}(r_\parallel, r'_\parallel) &= \sum_{gg'} (G^{-1}_{k_\parallel})_{gg'} e_g(r_\parallel, k_\parallel) e^*_{g'}(r'_\parallel, k_\parallel) \\ (G^{-1}_{k_\parallel})_{gg'} &= \left[C_{S^{\mathrm{L}}} \mathcal{G} C^\dagger_{S^{\mathrm{L}}}\right]^{-1} \\ \mathcal{G} &= \left[H + C^\dagger_{S^{\mathrm{R}}} (G^{-1}_{R,k_\parallel}) C_{S^{\mathrm{R}}} - EO\right]^{-1} . \end{aligned} \tag{15}$$

Repeating this procedure allows the evaluation of the embedding potential for an arbitrary stacking of atomic planes.

If the layers are identical and any parallel translation ($R_\parallel$) from layer to layer is incorporated within the embedding potential, the Hamiltonian and overlap matrices are unchanged. Thus the embedding potential with $n+1$ layers is related to that for n layers by

$$(G^{-1}_{\mathrm{R},k_\parallel})^{n+1} = E_{R_\parallel} \left[C_{S^{\mathrm{L}}} \mathcal{G}^n C^\dagger_{S^{\mathrm{L}}}\right]^{-1} E^\dagger_{R_\parallel} \tag{16}$$

where

$$\left[E_{R_\parallel}\right]_{gg'} = \delta_{gg'} \exp(\mathrm{i} g \cdot R_\parallel) . \tag{17}$$

Repeated iteration of (16) ultimately results in an embedding potential for a semi-infinite substrate. In effect the substrate is being assembled layer by layer, so although the procedure is guaranteed to converge (in the presence of a finite imaginary component in the energy), typically the addition of many hundreds of layers is needed. This is analogous to the construction of the reflection matrix in LKKR or the low-energy electron diffraction problem, where more efficient algorithms such as layer doubling are used to accelerate the convergence. Here, too, layer stacking does not constitute a practical algorithm for generating the embedding potential. However, we can develop a more efficient algorithm by defining

$$F^n = (G^{-1}_{\mathrm{R},k_\parallel})^n - E_{R_\parallel} \left[C_{S^{\mathrm{L}}} \mathcal{G}^n C^\dagger_{S^{\mathrm{L}}}\right]^{-1} E^\dagger_{R_\parallel} \tag{18}$$

so that $F^n = 0$ defines the semi-infinite embedding potential. If $F^n \neq 0$ then we determine a new estimate

$$(G^{-1}_{\mathrm{R},k_\parallel})^{n+1} = (G^{-1}_{\mathrm{R},k_\parallel})^n - D^n \tag{19}$$

such that

$$F^{n+1} = 0 . \tag{20}$$

Substituting (19) into (20) and retaining terms to first order in D^n gives

$$F^n = D^n - X^n D^n Y^n \tag{21a}$$

$$X^n = E_{\boldsymbol{R}_\parallel}\left[C_{S\mathrm{L}}\mathcal{G}^n C_{S\mathrm{R}}^\dagger\right]^{-1} \tag{21b}$$

$$Y^n = \left[C_{S\mathrm{R}}\mathcal{G}^n C_{S\mathrm{L}}^\dagger\right]^{-1} E_{\boldsymbol{R}_\parallel}^\dagger \tag{21c}$$

where (21*a*) may be solved by diagonalizing X^n and Y^n (Zhang *et al* 1989).

In figure 6 we compare the density of states obtained with the LKKR code and that calculated by embedding with the embedding potentials determined using this new algorithm. In this case, the system studied is a (100) Cu monolayer with embedding potentials describing semi-infinite (100) Cu substrates—in effect, bulk Cu. The density of states is evaluated at $\boldsymbol{k}_\parallel = (0.1, 0.2)$ au, the embedding plane half-way between layers and the various parameters as before. Once again there is striking agreement between these two completely independent calculations. The iterative solution to (18)–(21) was obtained with the zero matrix as the initial guess for the lowest energy, and for subsequent energies (interval 0.005 H) the embedding potential for the previous energy was the starting guess. We have found this to be the most efficient and stable procedure. As may be seen from figure 6, for most of the energy range only two iterations are necessary to converge the embedding potentials, and it is remarkable that halving the interval to 0.0025 H between successive energies reduces this to one—in effect, providing more information for no extra cost. The number of iterations required rises when the nature of the states in that energy range is changing rapidly. What differences exist between the LKKR result and the embedded monolayer calculation are probably due to the LAPW basis, in which only two basis vectors correspond to each of the four largest expansion vectors of the embedding potential. We have found that by using the the embedding potential obtained from the reflection matrix (equation (10)) as the initial guess, our algorithm converges to the same embedding potential as before but in *three* iterations (for all the energies considered), with the largest changes occurring in precisely those matrix elements. As a word of caution, on occasions our algorithm has failed to pick up the correct solution, converging to an embedding potential which results in unphysical charge distributions. However, this has only ever occurred when our initial guess has been particularly poor, such as the zero matrix within the d-band. We have also established that this algorithm can evaluate the embedding potential at energies with arbitrarily small imaginary components, with little increase in the number of required iterations, thus permitting extremely detailed analysis of surface states.

4. Closing remarks

We have described how one may use an embedding plane to simulate embedding on a more complicated surface, and demonstrated the accuracy of such a procedure. The benefits arise from greatly simplified matrix elements, which may be evaluated with the plane-wave part of the LAPW basis functions. In addition, the embedding potential is a property of the substrate, independent of the surface or interface to which it is coupled. Therefore, it need only be evaluated once for a given substrate geometry and energy wavevector, and for all subsequent uses it may be read in. It is a tremendous benefit to embed on a plane, as the expansion is compact.

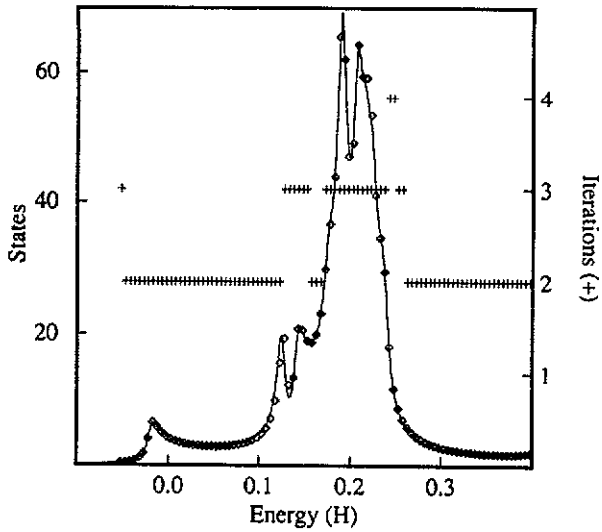

Figure 6. Muffin-tin density of states of bulk Cu at $k_{\parallel} = (0.1, 0.2)$ au (per spin-Hartree) with (100) taken as the perpendicular. The full curve is the result obtained with LKKR theory. The diamonds indicate values obtained by embedding a single (100) monolayer of Cu, the embedding potentials having been found using the iterative algorithm described in the text (equations (18)–(21)). The number of iterations required to converge the embedding potential, indicated by crosses, are also discussed in the main text. Calculation parameters and imaginary energy were identical to the Cu/Ni/Cu sandwich calculation.

We have, then, presented an algorithm for determining an embedding potential within the same framework as the subsequent evaluation of the surface or interface electronic structure. It is relatively easily implemented within the same program, and may be used to obtain an embedding potential with no shape approximation—unlike in previous applications of the embedding Green function method. The algorithm may be used to construct an embedding potential for an arbitrary arrangement of atomic planes—with the constraint that they possess the same in-plane periodicity—and in the case of a semi-infinite periodic substrate a particularly efficient iterative scheme has been described.

Even when the structural aspects of the surface or interface electronic structure problem are correctly treated, rather than approximated by slabs or supercells, the region of interest may contain a relatively large number of atoms. At a simple grain-boundary, for example, the electronic structure takes many atomic planes before it is bulk-like (Crampin *et al* 1989). With the straightforward application of the LAPW basis to this problem, the calculation time scales roughly with the cube of the number of atomic planes, since matrix inversion is an N^3 process. However, it is possible to obtain local information such as the charge density more efficiently, through the embedding procedure. Consider the region of interest partitioned into subvolumes, $i = 1, 2, \ldots, n+1$, shown in figure 7. A natural partitioning would assign one atomic plane to each subvolume, and at a surface the vacuum region would occupy one subvolume. The substrates have been removed and replaced by embedding potentials on S^{L} and S^{R}, in the case of a surface one of these being the free-electron or coulomb embedding potential, depending upon the treatment of exchange and correlation. We now use (15) to obtain the embedding potential for substrate + volume 1, on surface S^1 which

separates it from volume 2.

$$(G^{-1}_{\mathrm{L}1,k_\parallel})_{gg'} = \left[C_{S^1}\left[H_1 + C^\dagger_{S^\mathrm{L}}(G^{-1}_{\mathrm{L},k_\parallel})C_{S^\mathrm{L}} - EO_1\right]^{-1}C^\dagger_{S^1}\right]^{-1}. \tag{22}$$

Repeating, we can obtain all the necessary embedding planes for left embedding.

$$(G^{-1}_{\mathrm{L}i,k_\parallel})_{gg'} = \left\{C_{S^i}\left[H_i + C^\dagger_{S^{i-1}}(G^{-1}_{L(i-1),k_\parallel})C_{S^{i-1}} - EO_i\right]^{-1}C^\dagger_{S^i}\right\}^{-1}. \tag{22a}$$

The embedding planes for right embedding may be obtained by the reverse process, starting from the right substrate and adding additional volumes.

$$(G^{-1}_{\mathrm{R}n,k_\parallel})_{gg'} = \left\{C_{S^n}\left[H_{n+1} + C^\dagger_{S^\mathrm{R}}(G^{-1}_{R,k_\parallel})C_{S^\mathrm{R}} - EO_{n+1}\right]^{-1}C^\dagger_{S^n}\right\}^{-1} \tag{22b}$$

$$(G^{-1}_{\mathrm{R}i,k_\parallel})_{gg'} = \left\{C_{S^i}\left[H_{i+1} + C^\dagger_{S^{i+1}}(G^{-1}_{L(i+1),k_\parallel})C_{S^{i+1}} - EO_{i+1}\right]^{-1}C^\dagger_{S^i}\right\}^{-1}. \tag{22c}$$

These embedding potentials may then be used to embed the separate subvolumes and determine the charge density.

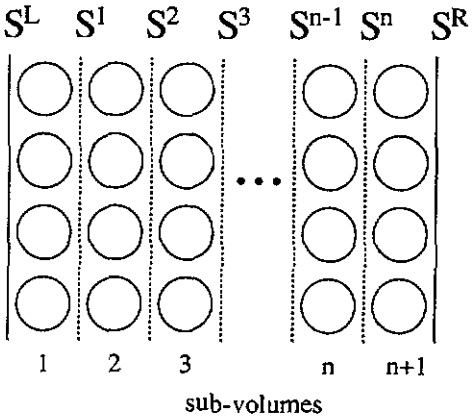

Figure 7. The atomic planes within the surface or interface region may be assigned to separate subvolumes, and treated independently via embedding potentials.

The benefit of this approach is that separate LAPW expansions may be made within each subvolume, and that the corresponding matrix inversions are performed on considerably smaller matrices. Incorporating an additional atomic plane, assigned to a new subvolume, does not increase the dimensions of the matrices to be inverted, and hence the approach has a linear scaling of the calculation time with the number of atomic planes. Of course one rarely gets something for nothing, and in this case the speed increase accompanies a loss of information. The off-diagonal elements of the Green function in the position representation are no longer available over the whole region, but only within each separate subvolume. In practice, this is information rarely used.

Acknowledgments

SC wishes to acknowledge the financial assistance of the Royal Society through the European Fellowship scheme.

References

Crampin S, Vvedensky D D, MacLaren J M and Eberhart M E 1989 *Phys. Rev.* B **40** 3413–416
Farquhar C P and Inglesfield J E 1989 *J. Phys.: Condens. Matter* **1** 599–610
Inglesfield J E 1981 *J. Phys. C: Solid State Phys.* **14** 3795–806
Inglesfield J E and Benesh G A 1988 *Phys. Rev.* B **37** 6682–700
MacLaren J M, Crampin S, Vvedensky D D and Pendry J B 1989 *J. Physique* B **40** 12164–75
Pendry J B 1974 *Low Energy Electron Diffraction* (London: Academic)
Pollmann J. and Pantelides S T 1978 *J. Physique* B **18** 5524–544
Skriver H L and Rosengaard N M 1991 *J. Physique* B **43** 9538–549
Zhang X-G, Rous P J, MacLaren J M, Gonis A, Van Hove M A and Somerjai G A 1990 *Surf. Sci.* **239** 103–118